JOURNAL OF SOLID STATE CHEMITRY 50, 100–110 (1983)

Simultaneous Measurements of Oxygen Pressure, Composition, and Electrical Conductivity of Praseodymium Oxides: I. Pr_7O_{12} and Pr_9O_{16} Phases

HIDEAKI INABA AND KEIJI NAITO

Department of Nuclear Engineering, Faculty of Engineering, Nagoya University, Furo-cho, Chikusa-ku, Nagoya, Japan

Received February 23, 1983; in revised form June 16, 1983

Simultaneous measurements of oxygen pressure, composition, and electrical conductivity have been made in the phases $Pr_7O_{12\pm x}$ and $Pr_9O_{16\pm x}$ and in the two-phase region. These two phases belong to the same homologous series with closely related structures of well-ordered oxygen vacancies. Composition–pressure, electrical conductivity–pressure diagrams suggest that the predominant point defects in these nonstoichiometric phases are neutral oxygen interstitials and doubly charged oxygen vacancies. The electrical conductivity–composition diagram does not follow Honig's model based on the assumption that Pr^{3+} and Pr^{4+} are randomly distributed in these praseodymium oxides. The electrical conduction in these praseodymium oxides is discussed on the basis of the hopping model with different mobilities of charge carriers, which come from the different sites of the ordered cation sublattice. Electrical conductivity–composition diagrams as well as oxygen pressure–composition diagrams show a reproducible hysteresis loop that is discussed in terms of a domain model.

1. Introduction

The praseodymium oxides belong to a fluorite-related homologous series Pr_nO_{2n-2} of intermediate phases with narrow ranges of nonstoichiometry and with ordered structures (*1–4*). The phase diagram of praseodymium oxide according to Hyde *et al.* (*1*) is shown in Fig. 1. Iota ($n = 7$) and zeta ($n = 9$) phases belong to this homologous series with ordered oxygen vacancies forming a superlattice and have the common *a* and *c* axes but a different *b* axis both in direction and in length (*2–4*).

The defect structure of the iota phase, $Pr_7O_{12\pm x}$, was discussed by Lau *et al.* (*5*) from the pressure dependence of the diffusion constant. The predominant defects were suggested to be neutral oxygen interstitials at low temperatures and a mixture of Frenkel defects with various charges at high temperatures. The intermediate praseodymium oxides consist of mixed valence cations, Pr^{3+} and Pr^{4+}, with partially filled 4*f* shells forming a narrow band. The electrical conductivity has been explained with a hopping mechanism and a small polaron theory (*6–9*). Honig *et al.* (*8*) found that the electrical conductivity of praseodymium oxides had a maximum around O/Pr = 1.75 and that the electrical conductivity of praseodymium oxides was proportional to the product of concentrations of Pr^{3+} and Pr^{4+} ions, $[Pr^{3+}][Pr^{4+}]$ (*8–10*).

The composition–pressure measurements between these intermediate phases

0022-4596/83 $3.00

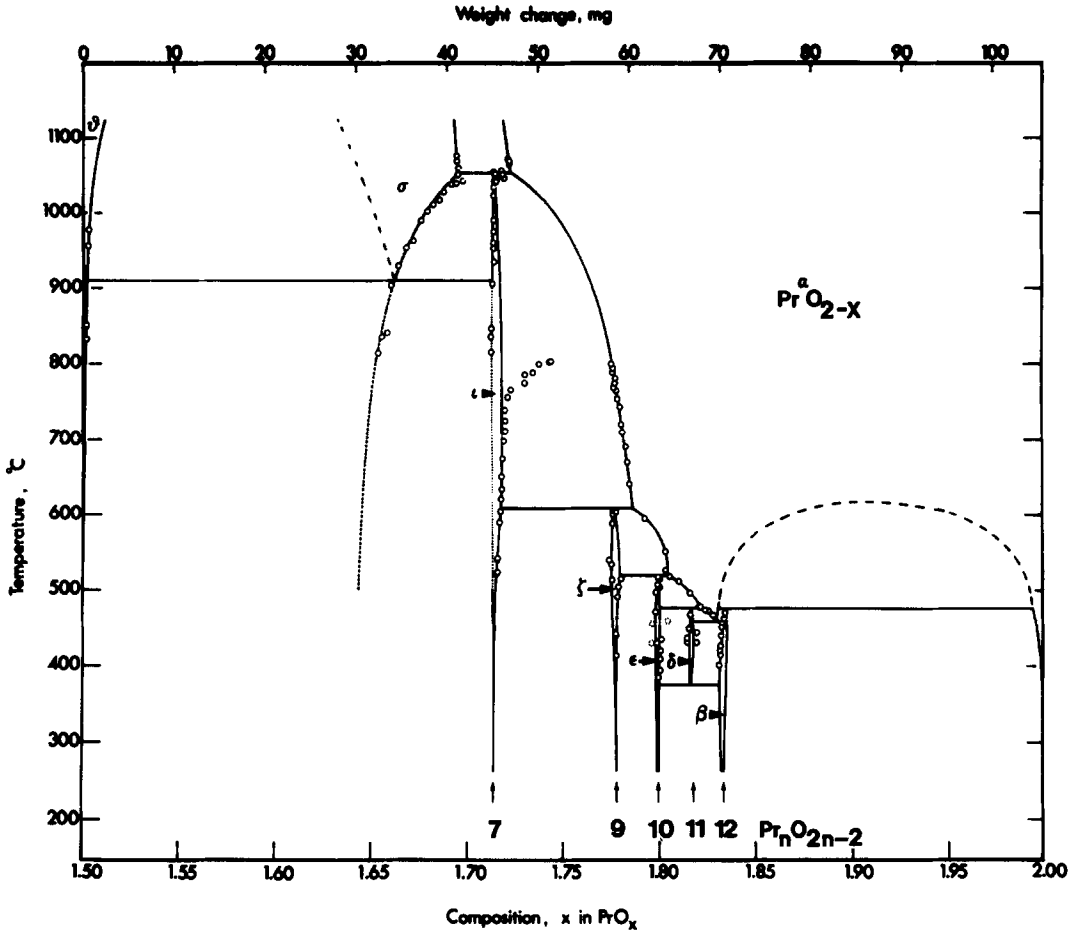

FIG. 1. Phase diagram of praseodymium oxides according to Hyde *et al.* (*1*).

have shown that reproducible hysteresis loops are found when the phase-reaction cycle is completed between two phases (*1, 11–15*). However, this kind of chemical hysteresis has been observed only in pressure–composition and the corresponding partial molar free energy–composition curves (*16*), while the measurements on other properties, such as the structure *in situ* and electrical conductivity along the hysteresis loop are needed to understand the nature and mechanism of hysteresis.

In this paper, simultaneous measurements of oxygen pressure, composition, and electrical conductivity have been made at high temperatures in the phases $Pr_7O_{12\pm x}$ and $Pr_9O_{16\pm x}$ and in the two-phase region. The defect structure, the electrical conduction, and the hysteresis in this system have been discussed, based on the results from the three simultaneous measurements.

2. Experimental

The oxygen vapor pressure and the corresponding O/Pr ratio were measured with a mercury manometer and the electrical conductivity was measured by the usual four-probe method, simultaneously. Five

pellets of praseodymium oxide were placed in a quartz sample tube and connected to a mercury manometer through a stopcock. Four platinum wire probes of 0.3 mm in diameter were inserted into one of the five pellets for the electrical conductivity measurement. The four platinum wires for electrical conductivity measurements and a Pt/Pt 13% Rh thermocouple of 0.3 mm in diameter for temperature measurement of the sample were led through holes in the sample tube and sealed with epoxy-type resin. The O/Pr composition in the sample was determined by calculating the change in moles of oxygen in the vapor phase by the use of the pressure change, and the predetermined dead volume of the apparatus. The dead volume of the sample tube was 29 cm^3 and that including one side of the manometer was about 95 cm^3. A correction of the volume was made due to the change of the manometer level. It was ascertained that no leakage occurred in the apparatus. The total weight of sample was 4.9832 g in the form of $PrO_{1.714}$. The sensitivity of the O/Pr ratio measurement is determined by the dead volume of the apparatus and the amount of the sample. A change in 100 Pa in oxygen pressure corresponded to about 0.002 units in O/Pr ratio. The precision of the composition measurement was estimated to be ± 0.0002 in the O/Pr ratio. The temperature of the sample was maintained constant within ± 1 K by using a stabilized power supply and adjusting the current of the electrical furnace manually.

The praseodymium oxide $Pr_{12}O_{22}$ with 99.99% purity was furnished commercially. The oxide was dissolved in 5 *N* HNO_3 and the solution was adjusted to 1 *N* HNO_3 by the addition of NH_3 gas. The oxalate, precipitated with oxalic acid, was washed and subsequently decomposed to the oxide by heating at 1273 K for 48 hr. The oxide so obtained was kept at 973 K and under an oxygen pressure of 133 Pa in order to obtain the iota phase.

3. Results

Simultaneous measurements of oxygen pressure, composition, and electrical conductivity were made for the iota phase ($Pr_7O_{12\pm x}$) along the oxidation and reduction paths in an isothermal condition at 973 K. The iota phase with the O/Pr ratio 1.714 is known to be obtained by equilibrating the sample at 973 K and 133 Pa of oxygen pressure (*1*). Composition–pressure and electrical conductivity–pressure relations are shown in Figs. 2 and 3, respectively, where the O/Pr ratio was determined relative to the deviation from 1.714, which is taken as a reference. It is seen from Fig. 2 that the nonstoichiometric parameter δ in $PrO_{1.714+\delta}$ takes both positive and negative values, indicating that the oxygen sublattice in iota phase has both interstitials and vacancies as defect species. The log σ vs log P plot in Fig. 3 forms a straight line in the oxygen pressure region below 4 kPa, with a slight positive slope of 0.005, but hysteresis between the oxidation and reduction paths is encountered in the region above 4 kPa. This

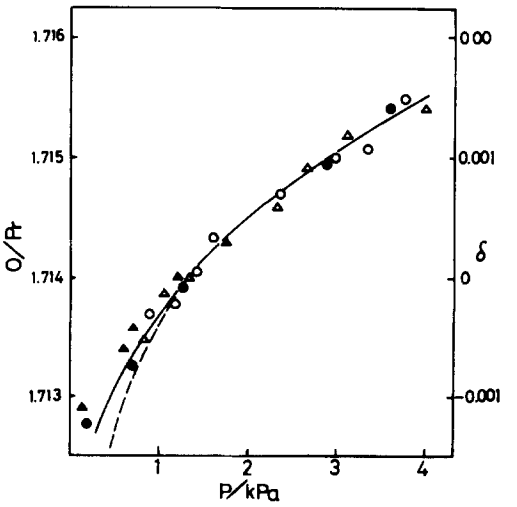

FIG. 2. Composition–pressure diagram in the iota phase $PrO_{1.714+\delta}$ at 973 K. ○, △ show the oxidation path and ●, ▲ the reduction path. The solid line represents the equation $\delta = K_1P^{1/2} - K_2P^{-1/6}$ and the broken line represents the equation $\delta = K_1P^{1/2} - K_2P^{-1/2}$.

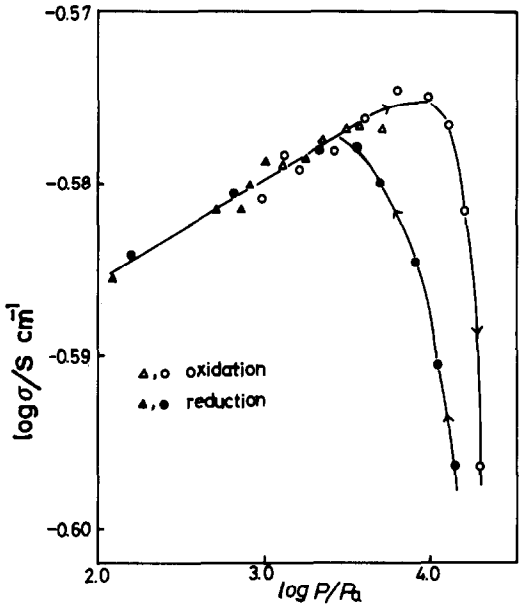

FIG. 3. Log vs log plot of electrical conductivity–oxygen pressure diagram near the iota phase at 973 K. ○, △ show the oxidation path and ●, ▲ the reduction path. The linear part of the plot can be expressed as $\sigma = \sigma_O P^{0.005}$.

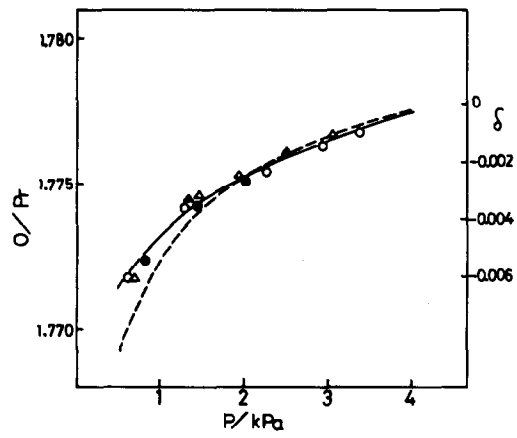

FIG. 4. Composition–pressure diagram in the zeta phase $PrO_{1.778+\delta}$ at 838 K. ○, △ show the oxidation path and ●, ▲ the reduction path. The solid line represents the equation $\delta = K_1P^{1/2} - K_2P^{-1/6}$ and the broken line represents the equation $\delta = K_1P^{1/2} - K_2P^{-1/2}$.

corresponds to the region of the two-phase mixture, Pr_7O_{12+x} and PrO_{2-x} (*16*) (see Fig. 1).

Simultaneous measurements of oxygen pressure, composition, and electrical conductivity were made for the zeta phase ($Pr_9O_{16\pm x}$) along the oxidation and reduction paths at 838 K. The reference O/Pr ratio was determined to be 1.714 at 838 K and at an oxygen pressure of 13.3 Pa, according to a previous study (*15*). Composition vs pressure and electrical conductivity vs pressure relations are shown in Figs. 4 and 5, respectively. Only a substoichiometric composition was obtained at this temperature and pressure below 4 kPa, as seen in Fig. 4. This is quite consistent with a previous thermogravimetric study (*15*). Figure 5 shows that a straight line in the log σ vs log P plot is obtained in the pressure region above 600 Pa, with a slight positive slope of 0.031. Hysteresis between oxidation and reduction paths is encountered in the region below 600 Pa, which corresponds to the region of the two-phase mixture, Pr_7O_{12+x} and Pr_9O_{16-x} (see Fig. 1).

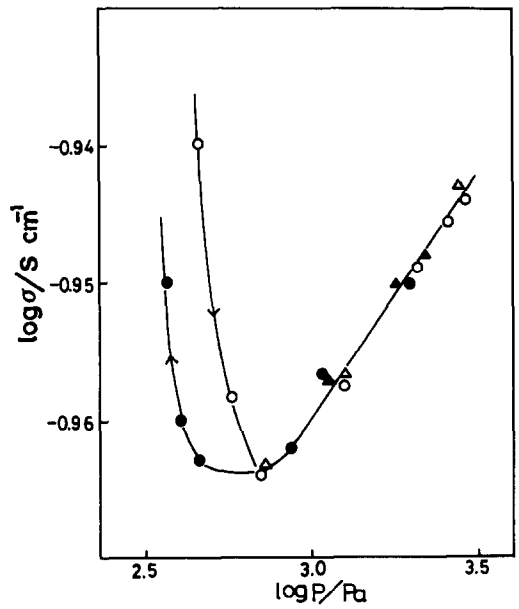

FIG. 5. Log vs log plot of electrical conductivity–pressure diagram near the zeta phase at 838 K. ○, △ show the oxidation path and ●, ▲ the reduction path. The linear part of the plot can be expressed as $\sigma = \sigma_O P^{0.031}$.

The results of simultaneous measurements at 838 K in the two-phase region between the iota and zeta phases are shown in Figs. 6 and 7. The pressure–composition curve, shown in Fig. 6, represents a reproducible hysteresis loop, in good agreement with the previous thermogravimetric study (*15*). The electrical conductivity–composition curve, given in Fig. 7, shows a somewhat strange behavior. The electrical conductivity increases with increasing O/Pr ratio in the nonstoichiometric iota phase, then decreases in the two-phase region, and finally begins to increase again in the nonstoichiometric zeta phase. Hysteresis in electrical conductivity is found in the two-phase region, as it is in the pressure–composition diagram shown in Fig. 6.

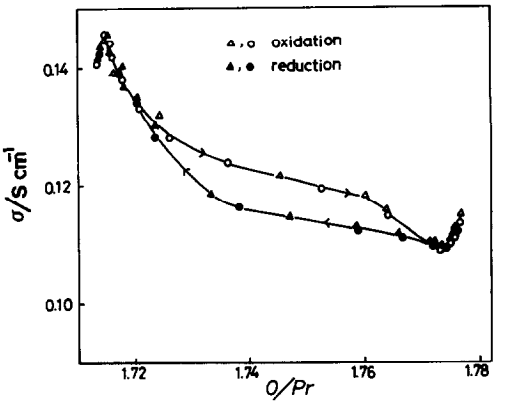

FIG. 7. Electrical conductivity–composition diagram along the hysteresis loop between the iota and zeta phases at 838 K. △, ○ show the oxidation path and ▲, ● the reduction path.

4. Discussion

4.1 The Defect Structure of the Iota ($Pr_7O_{12\pm x}$) and Zeta ($Pr_9O_{16\pm x}$) Phases

The unit cells for the iota and zeta phases have been determined by electron diffraction (*2*) as rhombohedral and triclinic, respectively, with two oxygen vacancies per unit cell, aligned along the $[21\bar{1}]$ axis of the fluorite sublattice. Figure 8 shows a structural model for the iota and zeta phases based on the results by Kunzmann and Eyring (*2*) projected along $[21\bar{1}]_F = [100]_\iota = [100]_\zeta$. The iota and zeta phases have common a and c axes, but have a different b axis in both direction and in length, as shown in Fig. 8.

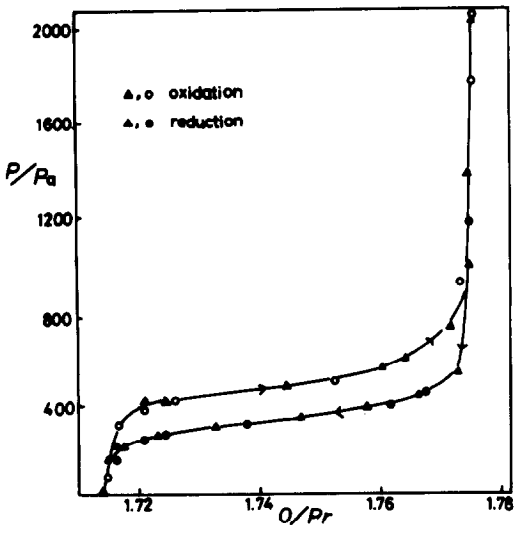

FIG. 6. Composition–pressure diagram along the hysteresis loop between the iota and zeta phases at 838 K. △, ○ show the oxidation path and ▲, ● the reduction path.

Interstitials and vacancies of oxygen atoms may be considered as a defect model for nonstoichiometric iota and zeta phases. Cations in the fluorite lattice form a FCC close-packed structure and interstitials and vacancies in cation sublattice would not easily be formed, compared with the mobile anion sublattice. Interstitials in the iota and zeta phases would mean the random occupation of the vacant positions marked with shaded or filled circles shown in Fig. 8. Lau *et al.* (*5*) discussed the defect structure of the nonstoichiometric iota phase ($Pr_7O_{12\pm x}$) from the oxygen pressure dependence of the diffusion constant. They considered neutral oxygen interstitials, doubly ionized oxygen interstitials, doubly ionized oxygen vacancies, and neutral oxygen vacancies as

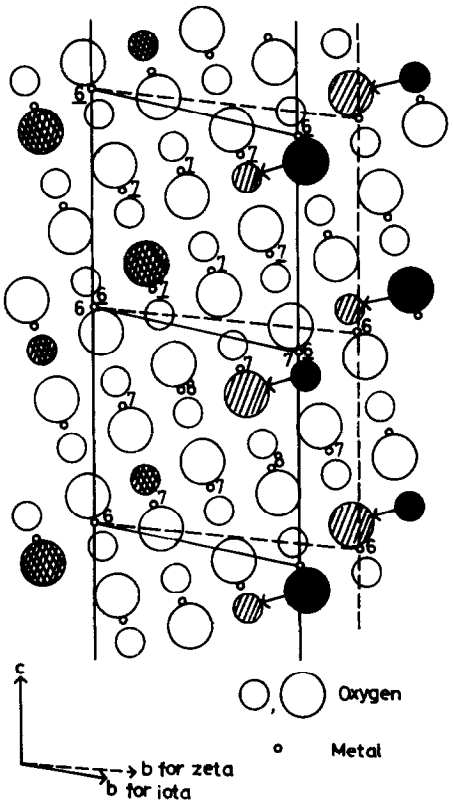

FIG. 8. A structural model for the iota (Pr_7O_{12}) and zeta (Pr_9O_{16}) phases. A projection along $[2\bar{1}\bar{1}]_F = [100]_\iota = [100]_\zeta$ is shown. Small circles represent rows of metal atoms; larger circles are rows of oxygen atoms, where the same size circle represents the same level. The circles shaded in one direction represent oxygen vacancies for the iota phase, and the filled circles represent oxygen vacancies for the zeta phase. The circles shaded in two directions are oxygen vacancies common to both the iota and zeta phases. The unit cells for the iota and zeta phases are shown in solid and broken lines, respectively. Numbers with and without an underline marked at metal positions represent the coordination numbers of cations for the iota and zeta phases, respectively.

point defects in the iota phase. The diffusion constant, assumed to be proportional to the concentration of point defects, was expressed as

$$D = \alpha_1 P_{O_2}^{1/2} + \alpha_2 P_{O_2}^{1/6} + \alpha_3 P_{O_2}^{-1/6} + \alpha_4 P_{O_2}^{-1/2}. \quad (1)$$

Based on this model, the oxygen pressure dependence of the diffusion constant was explained. At low temperatures (≈1017 K) the predominant point defects are neutral oxygen interstitials ($\alpha_2 = \alpha_3 = \alpha_4 = 0$) and at higher temperatures other terms become important. Considering the fact that electrical conductivity in the iota and zeta phases is nearly independent of the oxygen pressure, as seen in Figs. 3 and 5, neutral interstitials and vacancies are likely to be the predominant point defects in these phases. We introduce the nonstoichiometric parameter δ for $PrO_{1.714+\delta}$ and $PrO_{1.778+\delta}$,

$$\delta = [O_i] - [V_O] = K_1 P_{O_2}^{1/2} - K_2 P_{O_2}^{-1/2}, \quad (2)$$

where $[O_i]$ and $[V_O]$ are the concentrations of neutral oxygen interstitials and vacancies, respectively, and K_1 and K_2 are the equilibrium constants for the reactions

$$\tfrac{1}{2}O_2 = O_i, \quad (3)$$

$$O_O = V_O + \tfrac{1}{2}O_2. \quad (4)$$

The curve fitting of Eq. (2) to the experimental data is shown in Figs. 2 and 4 as broken lines. A good fit in the high pressure region is obtained, but a slight deviation is observed in the low pressure regions. To obtain a better fit, neutral oxygen interstitials and singly or doubly charged oxygen vacancies may be considered as the predominant point defects; these are also consistent with the diffusion study (*5*). Here we take neutral oxygen interstitials and doubly charged oxygen vacancies as the predominant point defects in the iota and zeta phases. Then,

$$\delta = [O_i] - [V_O''] = K_1 P_{O_2}^{1/2} - K_2 P_{O_2}^{-1/6}, \quad (5)$$

where K_2 is a constant in the reaction

$$O_O = V_O'' + \tfrac{1}{2}O_2 + 2e^-. \quad (6)$$

If the condition of the electroneutrality $2[V_O''] = [e^-]$ can be applied, then

$$[V_O''] \propto [e^-] \propto P_{O_2}^{-1/6}. \quad (7)$$

A better fit of Eq. (5) to composition–pressure curve is shown as solid lines in Figs. 2 and 4. According to Eq. (7), however, the electrical conductivity of the iota and zeta phases should be proportional to $P_{O_2}^{-1/6}$ in the substoichiometric regions, but the experimental data do not follow this law, as seen in Figs. 3 and 5. This matter will be discussed in the next section.

4.2 Electrical Conduction in Iota and Zeta Phases

(*a*) *Electrical conduction in stoichiometric compositions.* Honig *et al.* (*7*) measured Seebeck coefficients and electrical conductivities above 913 K over a wide range of the O/Pr ratio from 1.5 to 1.8 using a single crystal sample and found that the Seebeck coefficient changed the sign around $PrO_{1.75}$ from negative to positive as the O/Pr ratio increased and electrical conductivity became a maximum around $PrO_{1.75}$. According to their discussion (*8–10*), praseodymium oxides are *p*-type semiconductors in the region O/Pr < 1.75 and become *n*-type in the region O/Pr > 1.75. The electrical conductivity is proportional to the number of carriers (electrons or holes) and also to the number of sites into which the carriers can jump, on the basis of hopping mechanism and the assumption that Pr^{3+} and Pr^{4+} ions are randomly distributed. In this model,

$$\sigma = ne\mu \propto ns \propto [Pr^{3+}][Pr^{4+}] \propto (x - 1.5)(2 - x), \quad (8)$$

where n is the charge carrier density, e the charge carried on the electron, μ the charge carrier mobility, s the concentration of available sites to which the carrier can jump, $[Pr^{3+}]$ and $[Pr^{4+}]$ the concentrations of Pr^{3+} and Pr^{4+}, respectively, and x the O/Pr ratio of praseodymium oxide.

However, the following phenomena obtained by the present study seem to be different from the results by Honig *et al.* (*8*) and do not follow their model: (1) the compositional dependence of electrical conductivity, shown in Fig. 6, has a maximum at Pr_7O_{12+x}, then decreases as the O/Pr ratio increases, reaching a minimum at Pr_9O_{16-x}, and then begins to increase again, quite different from the behavior indicated by Eq. (8); (2) there is a small dependence of electrical conductivity on oxygen pressure in the $Pr_7O_{12\pm x}$ region as shown in Fig. 3 and a slightly positive dependence of electrical conductivity on oxygen pressure in the *n*-type $Pr_9O_{16\pm x}$ region as shown in Fig. 5.

The difference between the results by Honig *et al.* (*8*) and those by the present study may be due to the difference in temperature of the experiments; their results are obtained at 913 and 973 K where the iota and alpha phases are stable, while ours are obtained at 838 K where the iota and zeta phases are stable.

In the model by Honig *et al.* (*8*), the mobility of charge carriers is independent of site occupancy, since Pr^{3+} and Pr^{4+} ions are assumed to be randomly distributed in the praseodymium oxides. However, according to several structural studies (*3, 4*), Pr^{3+} and Pr^{4+} ions are ordered in the intermediate phases. The coordination numbers for the ordered metal positions in the iota and zeta phases can be obtained from the results by Von Dreele and Eyring (*4*) and Tuenge and Eyring (*3*), as marked at the metal positions in Fig. 8. For the stoichiometric compositions, praseodymium ions in one unit cell are composed of

$$Pr(6) \times 1 + Pr(7) \times 6 \quad (9)$$

for the iota phase (Pr_7O_{12}), and

$$Pr(6) \times 1 + Pr(7) \times 6 + Pr(8) \times 2 \quad (10)$$

for the zeta phase, where Pr(n) means a praseodymium ion surrounded by n O^{2-} ions; Pr(6) is thought to correspond Pr^{3+}, Pr(8), to Pr^{4+}, and Pr(7) corresponds either to Pr^{3+} or Pr^{4+}, and should be regarded as $Pr^{3.5+}$ as the average. As another formula-

tion of Pr_7O_{12} and Pr_9O_{16} we write

$$(Pr^{3+} \cdot Pr_6^{3.5+})O_{12}^{2-} \quad (11)$$

and

$$(Pr^{3+} \cdot Pr_6^{3.5+} \cdot Pr_2^{4+})O_{16}^{2-}, \quad (12)$$

respectively. It is believed that praseodymium ions form a narrow band and the electrical conduction in praseodymium oxides occurs via a hopping mechanism (*6–10*), i.e., the jumping of electrons or holes between Pr^{3+} and Pr^{4+} sites. As shown in Eqs. (9)–(12), there are three kinds of cation sites. Among these three sites, Pr(7) or $Pr^{3.5+}$ site would be the easiest site to jump to or from, because this site involves the variable valence Pr^{3+} or Pr^{4+}. Then, in a first approximation, the electrical conductivity of intermediate praseodymium oxides should be proportional to the concentration of Pr(7) in a unit volume. Since the numbers of Pr(7) in a unit cell are equal in Pr_7O_{12} and Pr_9O_{16} and since the unit cell volume of Pr_7O_{12} is smaller than that of Pr_9O_{12}, the electrical conductivity of Pr_7O_{12} is greater than that of Pr_9O_{16} as shown in Fig. 7.

Honig's model has provided a general explanation on the composition dependence of electrical conductivity and Seebeck effects of praseodymium oxides over a wide composition range. The present results show that in the intermediate phases, where both the cation and anion sublattices are ordered, the ordering effect in the cation sublattice and the contribution of point defects should be taken into account in the detailed analysis of the charges of electrical conductivity with composition and with oxygen pressures.

(*b*) *Electrical conduction in nonstoichiometric compositions.* The slightly positive slopes of the plot log σ–log P_{O_2} in both $Pr_7O_{12\pm x}$ and $Pr_9O_{16\pm x}$ phases can be interpreted in a manner similar to the preceding discussion, in that the concentration of Pr(7) is the main factor influencing the electrical conductivity, although $Pr_7O_{12\pm x}$ is thought to be *p*-type and $Pr_9O_{16\pm x}$, to be an *n*-type semiconductor, according to the Seebeck coefficient (*8*).

The predominant defects of hyperstoichiometric Pr_7O_{12+x} are thought to be neutral oxygen interstitials, judging from Fig. 2, and from the compositional dependence of diffusion constant. If one neutral oxygen atom is introduced per unit cell of Pr_7O_{12}, the change of cation sublattice may be expressed as

$$\text{Pr(6)} \times 1 + \text{Pr(7)} \times 6 \rightarrow \text{Pr(7*)} \times 1 + \text{Pr(7)} \times 5 + \text{Pr(8*)} \times 1, \quad (12)$$

where Pr(7*) is a praseodymium ion surrounded by six O^{2-} ions and one neutral oxygen atom, and Pr(8*) is a praseodymium ion surrounded by seven O^{2-} ions and one neutral oxygen atom. The charge in the cation sublattice remains constant in Eq. (12), and this would be a reason for the very small slope of the log σ vs log P_{O_2} relationship in Fig. 3. The decrease in concentration of Pr(6) and the increase in concentration Pr(7*) is also represented properly in Eq. (12). The charge of Pr(7*) would be mostly Pr^{3+}, but this cation is more likely to be involved in the charge exchange between Pr^{3+} and Pr^{4+} ions than Pr(6), because the seventh adjacent neutral oxygen is more electronegative and is apt to attract electrons from the Pr(7*) site. Therefore, neutral oxygen atoms would contribute to an increase in the electrical conductivity by increasing the probability of hopping.

As noted in the preceding section, if we use the band model, the slope in the log σ vs log P_{O_2} plot in hypostoichiometric Pr_9O_{16-x} should be $-\frac{1}{6}$ according to Eqs. (5)–(7), whereas the experimental result in Fig. 5 shows a small positive value of 0.031. The electrons ascribed to the doubly charged oxygen vacancies may be localized near the praseodymium ions according to the narrow band model (*5–9*), changing Pr^{4+} into Pr^{3+}. If one oxygen vacancy is

introduced in two unit cells of Pr_9O_{16}, the change of the cation sublattice may be given as

$$\mathrm{Pr(6)} \times 1 + \mathrm{Pr(7)} \times 6 + \mathrm{Pr(8)} \times 2 \rightarrow \mathrm{Pr(6)} \times 2 + \mathrm{Pr(7)} \times 6 + \mathrm{Pr(8)} \times 1, \quad (13)$$

and another corresponding expression is given as

$$(Pr^{3+} \cdot Pr_6^{3.5+} \cdot Pr_2^{4+})O_{16}^{2-} \rightarrow (Pr_2^{3+} \cdot Pr_6^{3.5+} \cdot Pr^{4+})O_{15.5}^{2-}. \quad (14)$$

No change in the concentration of Pr(7) is expected from Eqs. (13) and (14): this would be the main reason for a slight slope in the log σ vs log P_{O_2} plot in Fig. 5. The loss of oxygen ions in the oxide would change the electric field in the oxide and contribute to changes in the oxygen pressure dependence of electrical conductivity, but the reason for the decreasing dependence of electrical conductivity with decreasing pressure is not clear at present.

4.3 Chemical Hysteresis between the Iota and Zeta Phases

Chemical hysteresis between the oxidation and reduction paths in the rare earth oxides is a well-known phenomenon (*1, 11–15*). A thermodynamic model (*14*) based on the regular solution theory has been proposed for the hysteresis loop, in which the gross features of the main hysteresis loop are reproduced, but this model cannot account for the fact that truly constant oxygen pressure regions are never observed in pressure–composition measurements (*16*), as can be seen in Fig. 6. The thermodynamic model is based on the idea of metastability, i.e., the system continues to remain in a state corresponding to a free energy local minimum, even when that minimum is not the lowest one. The metastable states are formed by balancing the interfacial energy between the two phases with the mixing entropy of the two phases (*14, 16*). The necessity of the domain model has been stressed by Lin *et al.* (*17, 18*) in order to understand the nature of hysteresis more rigorously. Their model assumes that the distribution of domain sizes is the same for both the oxidation and reduction paths.

As seen in Fig. 7, the electrical conductivity σ shows a hysteresis loop, indicating that the distribution of domain sizes is different between the oxidation and reduction paths; this effect may be interpreted as follows: After showing a maximum in Pr_7O_{12+x}, σ rapidly decreases with increase of the O/Pr ratio by the oxidation because of the appearance of the zeta phase (in which σ is lower as compared with the iota phase), in the matrix of the iota phase, and because of scattering effects at the interface of the two phases. Close to $PrO_{1.74}$ the slope of the decreasing curve in σ becomes small up to the composition of roughly $PrO_{1.76}$, where the iota phase persists as a matrix, even though the volume fraction of iota phase is less than half. When the O/Pr ratio is increased above the $PrO_{1.76}$ composition, the iota phase no longer exists as a matrix, but rather as islands, and σ approaches the reduction path. Turning to the reduction path from the zeta phase, σ gradually increases with decrease of the O/Pr ratio because of the appearance of a highly conductive iota phase, but the scattering effect at the interface of the two phases suppresses the increase in σ. The gradual increase in σ persists up to the composition $PrO_{1.74}$, where the zeta phase exists as a matrix. When the O/Pr ratio is decreased below the composition $PrO_{1.74}$, the zeta phase no longer exists as a matrix and σ approaches the oxidation path. When we compare σ in the two-phase region (for example, at $PrO_{1.745}$), along the oxidation path and the reduction path, we see that the former is greater than the latter. The former phase is thought to be composed of islands of the zeta phase in a matrix of the iota phase and vice versa for the latter case, because σ

mainly reflects the electrical conductivity of the matrix component.

A model of domains is shown in Fig. 9, where the *B* phase extends in the same direction in the matrix of the *A* phase. This model is based on the experimental results (*19*) of the reduction of the zeta phase under the electron beam of the electron microscope, where the coherent intergrowth of iota phase is seen to occur in layers extending along the *c* direction common to the iota and zeta lattices. The parallel movements of vacancies, indicated by arrows shown in Fig. 8, would produce one layer of the iota phase from the matrix of the zeta phase. Nine layers of iota phase or seven layers of zeta phase result in the coherent intergrowth with the matrix of the zeta or the iota phase, respectively. This coherent intergrowth arises from the structural similarity between the iota and zeta phases and constitutes the main reason for hysteresis between the two phases.

From a thermodynamic point of view, the free energy of the system including the domain effect may be expressed by the sum

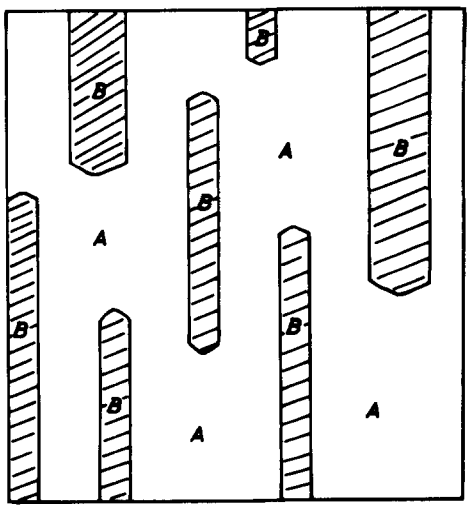

FIG. 9. A domain model for the texture of two-phase mixture in the hysteresis region. Islands of domains *B* coherently intergrow from the matrix phase *A*, extending in one direction.

of the chemical potential terms of domains *A* and *B*, the interfacial term between the domains *A* and *B*, the term due to size effect of domains, and the mixing entropy between the domains *A* and *B* (*18*). The presence of hysteresis may be explained as a metastable state involving a local minimum of the free energy, by balancing the interfacial term, the term due to size effect, and the mixing entropy. The domain model described in the present study assumes that the distribution of domains depends on the path. This assumption claims that the interfacial energy between domains also depends on the path, since the metastable state of a local minimum of free energy is determined by balancing the interfacial term, the term due to size effect, and the mixing entropy.

5. Concluding Remarks

(1) The electrical conductivities of nonstoichiometric $Pr_{17}O_{12\pm x}$ and $Pr_4O_{16\pm x}$ phases are found to increase very slightly with oxygen pressure, and the composition–oxygen relations for these phases are expressed by the relations $x = K_1P^{1/2} - K_2P^{-1/6}$. These are interpreted as indicating that the predominant point defects in these phases are neutral oxygen interstitials and doubly charged oxygen vacancies.

(2) The electrical conductivity has a maximum for the hyperstoichiometric iota phase (Pr_7O_{12+x}), decreases in the two-phase region as the O/Pr ratio increases, then has a minimum at a hypostoichiometric zeta phase (Pr_7O_{16-x}), and increases again in the nonstoichiometric zeta phase. These phenomena have been discussed on the basis of the hopping model with different mobilities of charge carriers, which derive from the different sites of the ordered cation sublattice. Among these sites the seven coordinated praseodymium ions are thought to play a major role in electrical conduction.

(3) The electrical conductivity–composition diagram, as well as the oxygen pressure–composition diagram, exhibits a reproducible hysteresis loop. The hysteresis is discussed on the basis of a domain model. The difference in electrical conductivity between the oxidation and reduction paths is interpreted as the difference in the domain structure, namely, the texture of a matrix of the *A* phase and islands of the *B* phase become reversed when the path is reversed.

(4) The electrical conductivity measurement on pressed pellets may include surface or grain boundary effects. In the present study, however, not only the electrical conductivity but also oxygen pressure and composition were measured simultaneously. The reproducibility of the electrical conductivity measurements was sufficiently good and the phase change, which represents a bulk property, was detected by the electrical conductivity measurements, as well as by the composition measurements. Therefore, it is believed that the electrical conductivity of the pressed pellets used in the present study mainly reflects the change of the bulk property.

Acknowledgment

The authors thank Dr. LeRoy Eyring, Professor of Chemistry, Arizona State University, for his valuable suggestions regarding the English usage and discussion of the manuscript.

References

1. B. G. Hyde, D. J. M. Bevan, and L. Eyring, *Philos. Trans. R. Soc. London Ser. A* **259,** 583 (1966).
2. P. Kunzmann and L. Eyring, *J. Solid State Chem.* **14,** 229 (1975).
3. R. T. Tuenge and L. Eyring, *J. Solid State Chem.* **29,** 165 (1979).
4. R. B. Von Dreele and L. Eyring, *Acta Crystallogr. Sect. B* **31,** 971 (1975).
5. K. H. Lau, D. L. Fox, S. H. Lin, and L. Eyring, *High Temp. Sci.* **8,** 129 (1976).
6. I. K. Naik and T. Y. Tien, *J. Phys. Chem. Solids* **39,** 311 (1978).
7. J. M. Honig, *J. Chem. Educ.* **43,** 76 (1966).
8. J. M. Honig, A. A. Cella, and J. C. Cornwell, *Rare Earth Res.* **2,** 555 (1964).
9. G. V. R. Rao, S. Ramdas, P. N. Mehrotra, and C. N. R. Rao, *J. Solid State Chem.* **2,** 377 (1970).
10. G. V. Vhandrashekhar, P. N. Mehrotra, G. V. Rao, E. C. Subbarao, and C. N. R. Rao, *Trans. Faraday Soc.* **63,** 1295 (1967).
11. D. A. Burnham and L. Eyring, *J. Phys. Chem.* **72,** 4415 (1968).
12. A. T. Lowe and L. Eyring, *J. Solid State Chem.* **14,** 383 (1975).
13. A. Lowe, K. H. Lau, and L. Eyring, *J. Solid State Chem.* **15,** 9 (1975).
14. D. R. Knittel, S. P. Pack, S. H. Lin, and L. Eyring, *J. Phys. Chem.* **67,** 134 (1977).
15. H. Inaba, S. P. Pack, S. H. Lin, and L. Eyring, *J. Solid State Chem.* **33,** 295 (1980).
16. H. Inaba, A. Navrotsky, and L. Eyring, *J. Solid State Chem.* **37,** 67 (1981).
17. J. A. Enderby, *Trans. Faraday Soc.* **51,** 835 (1955).
18. S. H. Lin, M. B. Langley, R. H. Langley, and L. Eyring, to be published.
19. L. Eyring, *in* "Nonstoichiometric Oxides" (O. T. Sørensen, Ed.), p. 337, Academic Press, New York, 1981.